18

Modeling of luminescence spectra in spherical microresonators with an emitting shell

© A.A. Dukin, V.G. Golubev

Ioffe Institute, St. Petersburg, Russia

e-mail: dookin@gvg.ioffe.ru

Received on May 09, 2021
Revised on June 16, 2021
Accepted on June 23, 2021

The luminescence spectra of a microresonator structure consisting of a spherical core of small diameter (3.5−6 mcm) covered with a luminescent shell with a refractive index less than that of the core are modeled. Shell luminescence spectra, radial distribution of the whispering gallery mode (WGM) field, and mode parameters (wavelength, width, quality factor) are calculated using the expansion of the electromagnetic wave field in the basis of vector spherical harmonics and the method of spherical wave transfer matrices. The dependence of the luminescence spectra and WGM parameters on the geometric and optical parameters of the structure — the shell thickness, the refractive index of the shell, and the core diameter — is studied.

Keywords: spherical microresonator, luminescent shell, whispering gallery modes, modeling of luminescence spectra.

DOI: 10.21883/EOS.2022.13.53986.2266-21

Introduction

Due to its unique optical properties spherical microresonators [1,2] attract a lot of attention in various optics areas [3–10]. Their unique properties are based on whispering gallery modes (WGM) — own modes of spherical microresonator electromagnetic field. Due to the total internal reflection, the WGMs are spreading along a curved microsphere inner surface in the form of a narrow ring along the equator. WGMs can have high quality factor, high energy density, long lifetime and low effective mode volume. Mode wavelengths and widths are determined by microsphere sizes, as well as by dielectric properties of microsphere and environment. In microspheres with a large diameter (tens and hundreds of microns) it is possible to obtain WGM with a very large quality factor, up to 10^{10} [11].

Microspheres with WGMs can be used in narrow-band filters in wavelength-division multiplexing systems, in femtosecond optical switches, in tunable optical delay systems, to create external optical feedback in lasers, to create optical waveguides from a number of closely-spaced microspheres, to focus radiation with subwavelength resolution using photonic jets [5,7].

An important field of application for microspheres with WGMs is sensorics. Large diameter microspheres (tens and hundreds of micrometers) can be used to detect the refraction index of the environment, chemicals, gases, biological substances, pressure, displacement, humidity, temperature, electric and magnetic fields, etc. [3,8,12–15]. Passive microresonators used as sensors require high-precision interfacing with signal input-output devices, such as optical waveguides, prisms, etc., which limits their application. Active microresonators (containing luminescent substances) used as sensors do not have this limitation, since the optical signal (WGM-modulated luminescence spectra) is excited and detected remotely, which makes it possible, for example, to introduce a microresonator into a living cell. In high-quality microresonators containing a laser medium, with sufficiently powerful optical pumping, it is possible to obtain laser radiation in a microsphere, which allows to reduce the width of the emission line, lower the limit of the adsorbed substance surface density detection [12], and also create compact and efficient low-threshold microlasers [6]. Low-threshold microlasers based on resonators with WGMs have been used for labelless detection of individual viral particles, detection of molecular electrostatic changes at biointerfaces, and for labeling and tracking live cells by barcode type [16,17].

The introduction of wide-band emitters into microresonators allows to simultaneously record a set of luminescence lines corresponding to WGM, and this can be used to increase the sensitivity of biological substances detection [18,19]. Light-emitting materials can be introduced either into the microsphere itself [20–23] or can be attached to its surface [24–32]. A light-emitting shell can also be applied on the microsphere surface [33] .

For microspheres of large diameter ($200\,\mu$m), the application of shell with a refraction index greater, than the refraction index of the microsphere itself allowed to increase the sensitivity of the sensors of environment refraction index and adsorbed particles [34]. Another way to increase the luminescent sensors sensitivity is to use small diameter microspheres — less than $10\,\mu$m [18,19].

The purpose of this study is to model the luminescence spectra of the microcavity structure consisting of a spherical core of small diameter ($3.5-6\,\mu$m) covered

with a luminescent shell with a refraction index lower, than that of the core. The shell luminescence spectra, the radial distribution of WGM field and the mode parameters (wavelength, width, quality factor) will be calculated using the electromagnetic wave field expansion in the basis of vector spherical harmonics and the method of spherical wave transfer matrices. The spectral dependence of the radiation intensity on the refraction index value, thickness and shell absorption value will be studied. The dependence of WGM parameters on structure geometric and optical parameters — shell thickness, shell refraction index, and core diameter will also be analyzed.

Microresonator structure under study and luminescence spectra modeling method

In the present study we will analyze core-shell spherical microresonators with a diameter less than $10\,\mu$m, in which a luminescent shell with a lower refraction index is applied on a spherical optically transparent dielectric core.

Microspheres of small diameter (less than $10\,\mu$m) with WGM can be used to determine the refraction index of the environment [35–37] and biomolecules [18,19,38]. In this case, the wavelength shift $\Delta\lambda$ and modes broadening are recorded, which occur due to the change of the environment refraction index n and/or adsorption on the microsphere surface of radius R of the analyzed substance. The sensor sensitivity is calculated as follows $\Delta\lambda/\lambda = \Delta R/R + \Delta n/n$, where λ — mode wavelength, ΔR and Δn — change of radius and refraction index respectively. Thus, the sensor sensitivity (line shift in the spectrum) is proportional to $1/R$ and increases with decreasing microsphere radius, which shows the advantage of using small diameter microspheres (up to several microns). Though in small diameter microspheres, due to the large surface curvature, the radiation losses are greater and, accordingly, the WGM quality factor is lower, than in the microspheres with a diameter of tens and hundreds of microns, the use of small diameter microspheres leads to a gain. In such microspheres, the increase in sensitivity compensates for the loss in resolution associated with mode broadening. An additional advantage of small diameter microspheres is the simplification of WGM spectrum due to the fact, that only modes with $q = 1$ remain in the spectrum and the intermode interval between them increases. This facilitates the identification of modes and allows to detect and analyze simultaneously a group of WGM lines in one spectrum [19]. It was demonstrated, that luminescent microspheres with a small diameter (approximately $2\,\mu$m) can detect only a few femtograms of the substance deposited on the surface of the microsphere [18]. Such a high sensitivity is associated both with a change in the microsphere radius and with a change of the refraction index due to the layer of substance adsorbed on the microsphere surface.

A spherical core can be synthesized from optically transparent amorphous silica (a-SiO_2) using the method described, for example, in [39]. The mesoporous shell can be made of densely packed tubes a-SiO_2 and have a system of monodisperse cylindrical pores with a controlled average diameter (1.5−3.5 nm) [40–42]. Such a shell can have a specific pore surface up to $1600\,m^2/g$, pores can occupy up to 60% of the shell volume. Due to porosity, the shell refraction index is less than the core refraction index, and the area of the chemically active surface of the pores, to which light-emitting particles and analyzed substances can be attached, is much greater, than the surface area of the microsphere of equal diameter. Thus, due to the developed network of interconnected pores and their large specific surface, the mesoporous shell can be filled with more light-emitting particles and analyte, than that, which can be attached to the sphere surface. In particular, the functionalization of mesoporous materials by broadband emitters, such as organic dyes [43–45] and carbon nanodots [46,47], has been demonstrated.

The advantage of nanoporous silica is the possibility of its use as a matrix for stabilizing the emission properties and spatial separation of luminophors, such as luminescent dyes [43,44], semiconductor quantum dots [48], oxides of rare earth elements [49], perovskite nanocrystals [50], carbon nanodots [46]. The luminescence brightness of such composite particles is mostly due to the spatial separation of luminophor molecules or nanoparticles inside silica particles, which reduces luminescence quenching. It is also demonstrated, that when luminophors, for example, carbon nanodots [51] or perovskite nanoparticles $CsPbBr_3$ [50,52] are introduced into nanoporous matrices, their radiative characteristics do not worsen and remain stable for a long time due to the decrease in the impact of external environment on the physical and chemical properties of the materials. The increase in the emission intensity of luminophores in the nanopores of silica matrices was achieved due to the plasmon interaction of luminophores with noble metal nanoparticles additionally introduced into the matrices pores [53].

It is important to note, that silica is an environmentally friendly and biocompatible material, and the technology of its production is cheap and scalable. It is known that nanoporous silica particles are non-toxic, able to penetrate through the cell membrane and accumulate in cells. Coating the particles surface with specific ligands ensures their targeted delivery to cells due to ligand-receptor interaction. This method is widely used when creating multifunctional systems for theranostics of oncological diseases based on nanoporous silica. Thus, using multifunctional systems for theranostics, which use composite particles based on nanoporous silica, it is possible to carry out diagnostics, high-tech therapy, targeted delivery of toxic chemotherapy drugs without harming healthy body tissues, to monitor drug delivery and the results of therapy [54–56]. The possibility of creating microresonators and microlasers from composite materials based on nanoporous silica opens up prospects for studying intracellular processes *in vitro* and *in vivo*.

To simulate the luminescence spectra in microresonators, we used the method of calculating the emission spectra of dipoles located in a spherical layer [57]. The cited study considered the structure consisting of a central spherical core and a multilayer system of concentric spherical layers surrounding it. In one of the structure layers there are radiating dipoles. Given the spherical symmetry of the problem, Maxwell's equations are considered in spherical coordinates. The electromagnetic field in each spherical layer is the sum of the field created by the dipoles in a given layer and the field penetrating from adjacent layers through the boundaries. The electromagnetic wave field is expanded in the basis of vector spherical harmonics. The electromagnetic field in such a basis has two polarizations (TE and TM). The field with TE-polarization does not have a radial component of the electric field, the field with TM-polarization does not have a radial component of the magnetic field (Fig. 1, *a*). The continuity conditions for the tangential components of the electric and magnetic fields at each spherical interface between two adjacent layers make it possible to relate the amplitudes of the electric and magnetic fields in adjacent layers using a transfer matrix through this interface.

In this study we simulated the emission spectra of a luminescent shell deposited on an optically transparent spherical dielectric core. The transfer matrix for the entire structure is obtained by multiplying the transfer matrices for the outer boundary of the shell and the boundary between the shell and the core. It links the fields amplitudes in the core and environment, taking into account the radiation created by the dipoles located inside the shell. The intensity radiated outward from the shell filled with randomly oriented dipoles is calculated using the transfer matrix. Thus, the spherical shell filled with emitters, such as nanodots, molecules or atoms, is modeled. Using the field expansion in the basis of vector spherical harmonics, the spatial distribution of fields inside and outside the structure is calculated. All calculations were made using the Mathematica software package.

The wavelengths of the eigenmodes of the electromagnetic field in this structure are calculated from the condition, that the transfer matrix for the entire structure is equal to zero. These modes have an asymptotics in the form of a spherical wave running away at infinity and are characterized by three numbers: polar index l ($l \geq 1$), azimuthal index m ($-l \leq m \leq l$), radial index q and two polarizations (TE and TM). The polar index l and the azimuthal index m describe the angular distribution of the field (the number of mode maxima in the equatorial section is $2|m|$, the number of mode maxima in the meridional section is $l - |m| + 1$). The radial index q corresponds to the number of the mode maxima lying inside the structure along the radius. Figure 1, *b* shows the characteristic distribution of the electric field strength along the radial coordinate for a TE-polarized WGM with $q = 1$ on a schematic representation of modeled structure section. Mode frequencies do not depend on m, i.e. the modes are multiply degenerate in m. For whispering gallery modes $m = l$ or m is close to l, and the value q does not exceed a few units [1]. Further WGMs will be denoted as TE_l^q or TM_l^q, where TE and TM are WGM polarizations, q and l — corresponding indices.

Results and discussion

Figure 2 shows the emission spectra of the luminescent shell deposited on a spherical core. In this figure and in the figures below, the dipole radiation intensity inside the shell is normalized to the dipole radiation intensity in a homogeneous medium, in which the values of the relative permittivity and permeability are equal to those in the shell. Figure 2, *a* shows the emission spectra of the shell separately for the TE and TM radiation polarizations. For each polarization the spectrum consists of a large number of ordered peaks. The WGM designations are given above the peaks. All peaks in the spectrum correspond to the WGM with the radial index $q = 1$. The polar mode indices of adjacent peaks for each polarization differ by one. The amplitude of the peaks increases monotonically, while the width decreases monotonically as the polar index l increases. The peak amplitude for TE-polarized WGMs is somewhat larger, and the width is somewhat smaller, than for TM-polarized WGMs with the same polar and radial indices [58].

Figure 2, *b* shows the emission spectra of the shell, including both TE and TM polarizations. The wavelengths for TM-polarized modes are close to the wavelengths of TE-polarized modes with the same indices l and q, so the peaks strongly overlap in the emission spectrum of the total (unpolarized) radiation (curve *1*, Fig. 2, *b*). WGMs are localized inside the structure in the form of the narrow ring adjacent from the inside to the outer shell surface. The wave propagates along this boundary with the environment and due to the total internal reflection from it. The mode width decreases as the optical contrast increases (the ratio of refraction indices of the cladding and the environment) due to the increase in the reflection coefficient from this boundary with the environment. This is due to the decrease in radiation losses upon reflection from the boundary and an increase in the lifetime of a photon inside the structure. In this case the narrowing of the peaks can be achieved by increasing the refractive index of the shell (curve *2*, Fig. 2, *b*). Besides, the WGM width decreases as the core radius increases [2]. This is due to the fact, that as the radius increases, the curvature of the boundary along which the WGM wave propagates decreases, and as a result, the radiative losses decrease. Thus, as the core radius increases, the lines also narrow and are better separated (curve *3*, Fig. 2, *b*). Line narrowing depends on shell parameters, which will be discussed further. On all three spectra in Fig. 2, *b* the spectral positions of the modes TE_{27}^1 and TM_{27}^1 are designated. It is seen, that as the shell refraction index

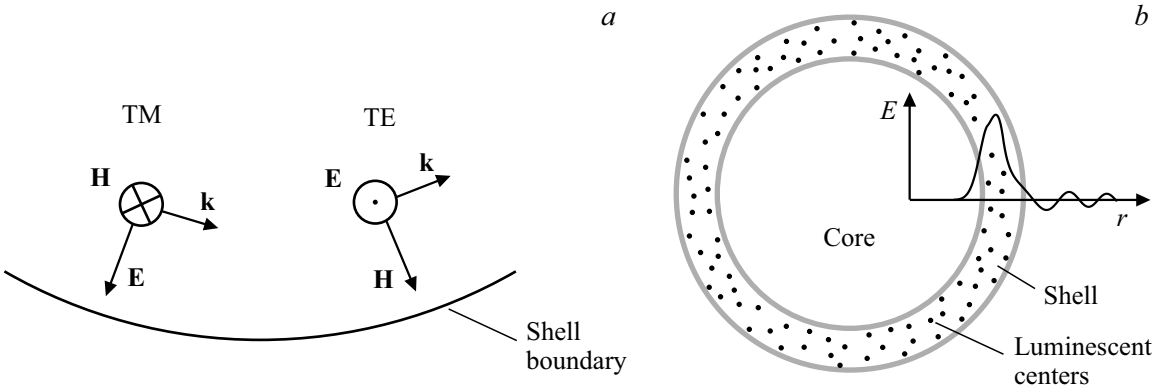

Figure 1. (a) The image of electric field **E**, magnetic field **H** and wave vector **k** for TE- and TM-polarized whispering gallery modes and fragment of the boundary between shell and environment. (b) Schematic representation of the simulated structure section: two concentric circles show the shell boundaries, a graph is superimposed on them showing the characteristic distribution of the electric field strength (E) along the radial coordinate (r) for TE — polarized WGM with $q = 1$. Dots indicate luminescent centers in the shell.

and the core diameter increases, the position of WGM peaks in the spectra shifts to the long-wavelength region.

In the case of a porous shell, when the pores are filled, for example, with both luminescent materials and analyzed materials adsorbed from the environment, the refraction index of the shell increases. Therefore, it is of interest to study the change in WGM spectra with an increase in the refraction index of the shell. Since in this study we consider only shells with a refraction index less than that of the core, we should initially analyze the limiting case, when the refraction index of the shell is equal to the refraction index of the core.

Figure 3 shows the emission spectra of 300 nm luminescent shell with a refraction index of 1.46, deposited on the 3.5 μm core with a refraction index of 1.46. The radiation intensity is given on a logarithmic scale in order to show low intensity peaks corresponding to modes with $q = 2$. Compared to the shell of the same thickness, but with a lower refraction index 1.21 (Fig. 2, b), the peaks are shifted to the long-wavelength region, the widths of the modes with $q = 1$ decreased, and as a result TE- and TM-polarized lines do not overlap. For example, for the modes $l = 27$, $q = 1$, the wavelength $\lambda(\mathrm{TE}_{27}^1)$ increased from 520.3 nm to 590.4 nm, the quality factor (Q) increased from 350 to 3830, the width decreased from 1.49 to 0.154 nm. The difference between the wavelengths of TE- and TM-polarized WGMs with the same indices $\lambda(\mathrm{TE}_{27}^1) - \lambda(\mathrm{TM}_{27}^1)$ increased from 4.1 to 11.5 nm. A decrease in WGM width and, as a consequence, an increase in quality factor occurs due to the increase in the optical contrast, as was noted earlier when discussing Fig. 2. The total number of WGMs in the considered spectral interval increased, while the intermode interval decreased. This is explained by the fact, that due to the increase in the refraction index of the shell, the optical length of the path along which the WGM runs inside the resonator increased [6].

In addition, in the short-wavelength part of the spectrum with refraction index of the shell 1.46, a group of lines linked to the modes with $q = 2$ appeared. Their appearance in the spectrum is due to the decrease in the width of these modes and the increase in the amplitude of the corresponding peaks as a result of optical contrast increase (see the discussion of Fig. 2). Modes with $q = 2$ have shorter wavelength, much lower quality factor (Q) and peak amplitude (A): $\lambda(\mathrm{TE}_{27}^2) = 515.5$ nm, $Q(\mathrm{TE}_{27}^2) = 168$, $A(\mathrm{TE}_{27}^2) = 0.221$ compared to the modes with $q = 1$ and the same polar index l, namely $\lambda(\mathrm{TE}_{27}^1) = 590.4$ nm, $Q(\mathrm{TE}_{27}^1) = 3830$, $A(\mathrm{TE}_{27}^1) = 19.9$. Thus, an increase in the refraction index of the shell leads to a decrease in the width and an increase in WGM quality factor, to a mode shift to the long wavelength region of the spectrum, to an increase in the number of WGMs in the selected spectral range, and to the appearance of modes with $q = 2$.

In order to understand how an increase in the core diameter affects the WGM spectrum, the emission spectra of 300 nm shells with refraction indices 1.21 (Fig. 4, a) and 1.46 (Fig. 4, b) deposited on a 6 μm core were calculated. Compared to 3.5 μm (Fig. 2, a) core diameter the number of modes with $q = 1$ in the spectral range 550–650 nm has increased from 8 to 14. An increase in the core diameter also led to an increase in the wavelength and WGM quality factor. So, for example, for the TE_{27}^1 mode, the wavelength increased from 520.3 to 882.8 nm, and the quality factor increased from 350 to 1560 correspondingly. With an increase in the resonator size, the intensity of the normalized luminescence peaks increases, so, for example, for TE_{27}^1 mode, the peak amplitude increased from 1.04 to 7.2.

In the entire studied spectral range 550–650 nm, there are not only modes with $q = 1$, but also modes with $q = 2$ with both TE and TM polarizations. In this case, the peaks of the modes of TE- and TM-polarizations with $q = 1$ do not overlap, while the peaks of the modes of TE- and TM-polarizations with $q = 2$ overlap considerably. The quality factor and peak amplitude of modes with $q = 1$ are approximately two orders of magnitude greater, than the

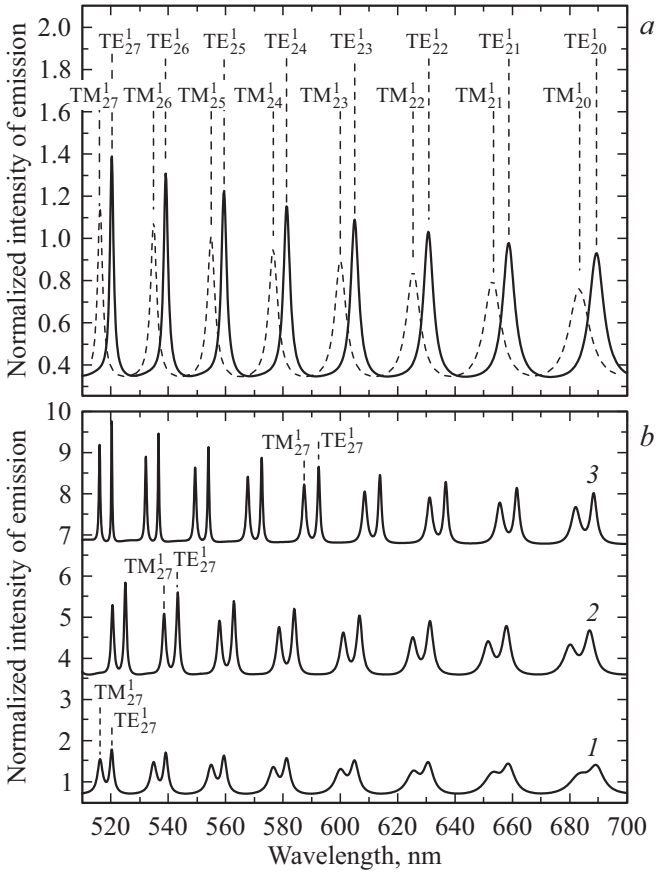

Figure 2. Spectral dependences of the radiation intensity of the luminescent shell surrounding the spherical core. The refraction index of the core is 1.46, the shell thickness is 300 nm. (*a*) Solid line — TE polarization, dashed line — TM polarization, core diameter 3.5 μm, shell refraction index 1.21. (*b*) Unpolarized radiation spectra: *1* — shell refraction index 1.21, core diameter 3.5 μm; *2* — shell refraction index 1.31, core diameter 3.5 μm, spectrum shifted up; *3* — shell refraction index 1.21, core diameter 4 μm, spectrum shifted up. Vertical dashed lines indicate WGM positions. Mode designations are indicated next to the vertical lines.

quality factor and peak amplitude of modes with $q = 2$ for the same polarizations and polar indices l.

In the narrower spectral range Figure 4, *b* shows the emission spectra of 300 nm luminescent shell with a refraction index of 1.46, surrounding 6 μm core with a refraction index of 1.46. It can be seen, that compared to the shell with a refraction index of 1.21 (Fig. 4, *a*), the amplitudes of WGM peaks with $q = 1$ and $q = 2$ increased by more than an order of magnitude. Moreover, TE- and TM-polarized modes with $q = 2$ do not overlap. The quality factor of modes for the shell with a refraction index of 1.46 also increases by several times, compared to the quality factor of modes for the shell with a refraction index of 1.21, which have the same polarization and the same indices. The limiting value of the quality factor for WGM with the given values of the polar and radial indices at a fixed outer shell radius is determined by the maximum possible refraction index of the shell. Since in this study we consider only the shells with a refraction index less, than that of the core, the maximum possible refraction index of the shell is the refraction index of the core. Accordingly, the maximum achievable value of WGM quality factor is the WGM quality factor in a homogeneous ball with a radius equal to the outer radius of the shell and a refraction index equal to the refraction index of the core. So, for the TE^1_{27} mode, the limiting quality factor is $Q = 3830$ in the structure with a 3.5 μm core, refraction index 1.46, and shell thickness 300 nm with a refraction index of 1.46. This quality factor is reduced, for example, by absorption in the shell material. The influence of absorption on the luminescence spectra is considered below.

Let us consider the dependence of WGM parameters on the shell thickness. For this, a structure was chosen in which a core 3.5 μm in diameter with a refraction index of 1.46 is surrounded by a shell with a refraction index of 1.31. The shell thickness varies from 1 to 800 nm. For such a structure, the spectral dependences of the radiation intensity of the shell (Fig. 5), the WGM electric field distribution along the radial coordinate (Fig. 6), and the parameters (wavelength, mode width, quality factor) of the TE and TM modes (Fig. 7) were calculated at different values of the shell thickness.

Figure 5 shows the spectral dependences of the radiation intensity from the luminescent shell. The vertical arrows mark the spectral positions of the TE^1_{27} and TM^1_{27} modes. It can be seen, that as the shell thickness increases, the WGM wavelengths with a constant polar index l shift to

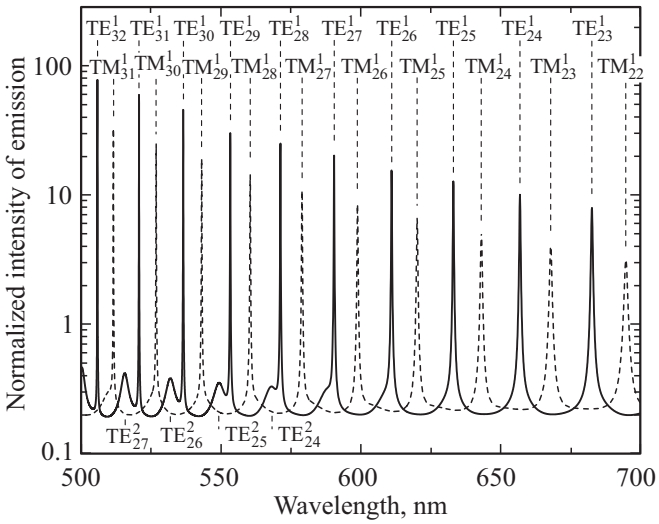

Figure 3. Spectral dependences of the radiation intensity of a luminescent shell with a thickness of 300 nm and refraction index of 1.46, surrounding a core with a diameter of 3.5 μm and refraction index of 1.46. Solid line — TE polarization, dashed line — TM polarization. Vertical dashed lines indicate WGM positions. Mode designations are indicated next to the vertical lines.

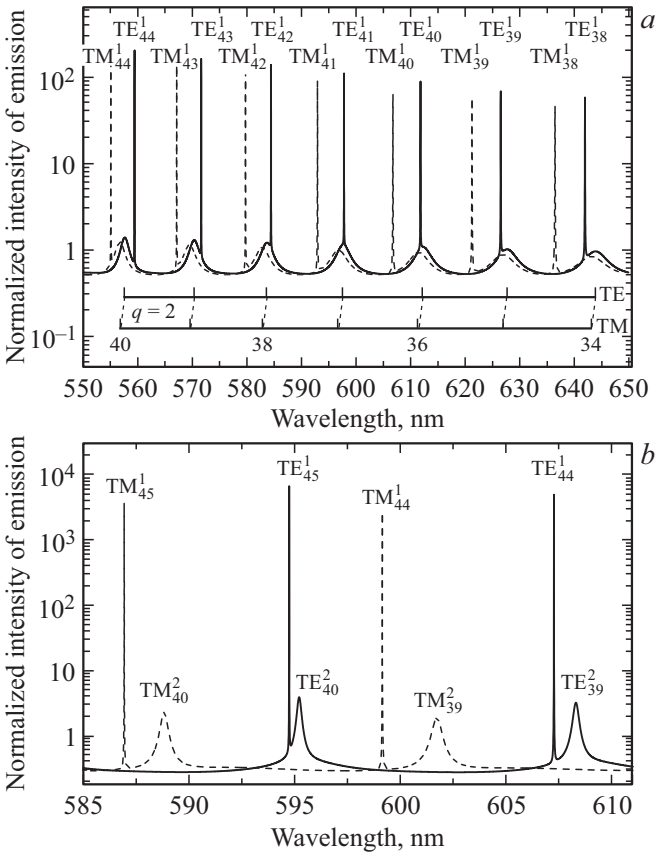

Figure 4. Spectral dependences of the radiation intensity of a luminescent shell with a thickness of 300 nm surrounding a core with a diameter of 6 μm and refraction index of 1.46. Solid lines — TE polarization, dashed lines — TM polarization. (*a*) Shell refraction index 1.21. (*b*) The refraction index of the shell is 1.46. The WGM designations are indicated above and below the peaks.

longer wavelengths, the peaks broaden, and their amplitude decreases.

Figure 6 shows the calculated distribution of the TE^1_{27} mode electric field strength along the radial coordinate for different values of the shell thickness in the range from 1 to 800 nm. The distribution plot of the electric field strength for the TM^1_{27} mode repeats the main features of the distribution plot for the TE^1_{27} mode, and therefore is not given. Inside the structure, the WGM field propagates as a running wave, which experiences total internal reflection from the outer shell boundary; outside the outer boundary there is a small area of an evanescent, exponentially decaying field, which then turns into a spherical wave running away to infinity. Since the WGM field is pressed against the outer structure boundary, then as the shell thickness increases, this maximum shifts to the region of large values of the radial coordinate. In the thickness range of 1−200 nm, the maximum of the electric field is inside the core, within the thickness range of 300 nm and more, the maximum is inside the shell. For a shell thickness of 250 nm, the field maximum passes from the core to the shell. With a shell thickness of 800 nm and more, practically the entire WGM field is concentrated inside the shell. In this case, WGMs are very close to the modes of a homogeneous sphere with a refraction index equal to that of the shell and with a sphere radius equal to the outer shell radius.

Figure 7 shows the calculated wavelength, mode width, quality factor, and relative wavelength difference $[\lambda(TE^1_{27}) - \lambda(TM^1_{27})]/[(\lambda(TE^1_{27}) + \lambda(TM^1_{27}))/2]$ for two modes TE^1_{27} and TM^1_{27} with the same constant polar and radial indices depending on the shell thickness. As the shell thickness increases, the WGM wavelength with given indices increases monotonically. In this case, in the thickness ranges 50−200 nm and 500−800 nm, the

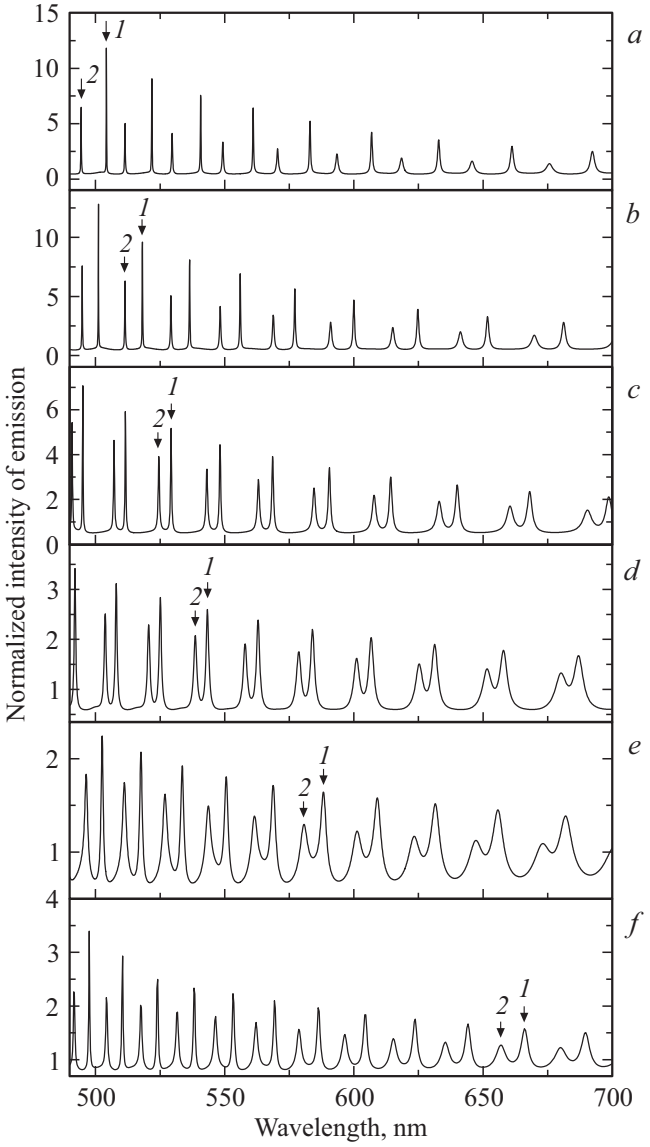

Figure 5. Spectral dependences of the radiation intensity of a luminescent shell with refraction index of 1.31, surrounding a core with a diameter of 3.5 μm and refraction index of 1.46. Shell thickness: *a* — 1, *b* — 100, *c* — 200, *d* — 300, *e* — 500, *f* — 800 nm. The vertical arrows *1* and *2* denote the spectral positions of the whispering gallery modes TE^1_{27} and TM^1_{27} correspondingly.

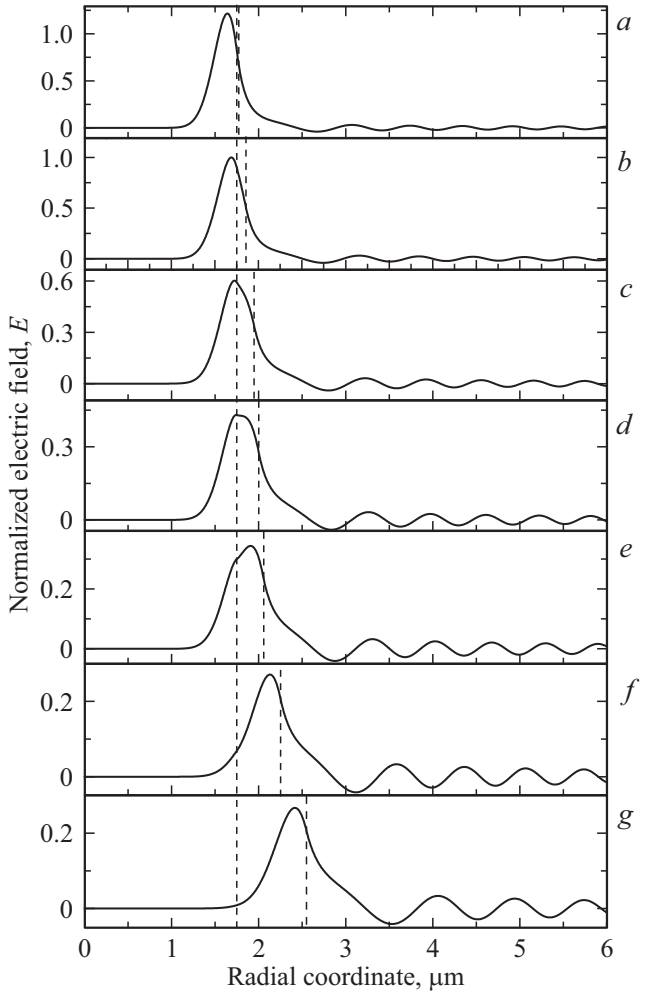

Figure 6. Electric field strength distributions of the whispering gallery mode TE_{27}^{1} in a microresonator structure along the radial coordinate. A shell with a refraction index of 1.31 is deposited on 3.5 μm core with a refraction index of 1.46. Shell thickness: *a* — 1, *b* — 100, *c* — 200, *d* — 250, *e* — 300, *f* — 500, *g* — 800 nm. Vertical dashed lines show the boundaries of the shell with the core and the environment. The field profiles are normalized, so that the amplitude of the runaway wave is 1.

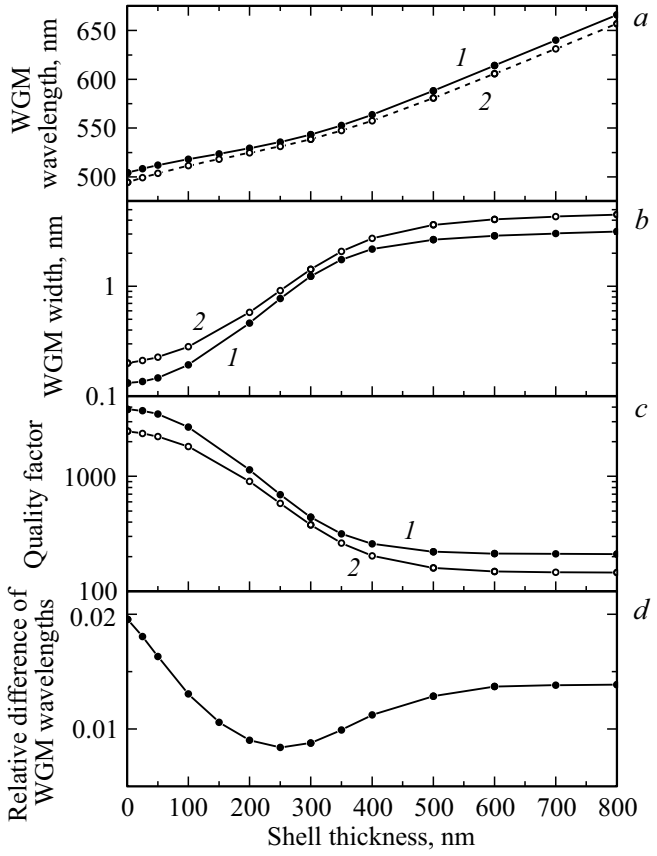

Figure 7. Dependences of the wavelength (*a*), width (*b*), quality factor (*c*) of the whispering gallery mode TE_{27}^{1} (*1*) and TM_{27}^{1} (*2*) on the shell thickness; (*d*) — dependence of the relative wavelength difference of whispering gallery modes TE_{27}^{1} and TM_{27}^{1} $[\lambda(TE_{27}^{1}) - \lambda(TM_{27}^{1})]/[(\lambda(TE_{27}^{1}) + \lambda(TM_{27}^{1}))/2]$ on the shell thickness. A shell with a refraction index of 1.31 is deposited on a 3.5 μm core with a refraction index of 1.46.

wavelengths depend almost linearly on the shell thickness, but the dependences have a different slope. This can be explained by the fact, that in the thickness range 0–200 nm the WGM electric field maximum lies inside the core, and the core makes a decisive contribution to WGM formation. In the range of the thicknesses more than 500 nm, the maximum of the electric field of the modes lies inside the shell, and the shell makes a decisive contribution to WGM formation.

The peak width of both TE and TM polarized modes increases monotonically as the shell thickness increases (Fig. 7, *b*). In addition, the amplitudes of the field radial distribution maxima (Fig. 6) and amplitudes of peaks (Fig. 5) decrease monotonically as the thickness grows. This can be explained as follows. At very small values of the shell thickness, its influence can be considered insignificant and it can be assumed that during WGM propagation, reflection occurs from the boundary between the core and the environment — air. The optical contrast and, accordingly, the reflection coefficient for the core-air boundary is greater, than for the shell-air boundary. Therefore, for a negligibly small shell thickness, the WGM width is minimal, while the quality factor, the peak amplitude in the radiation intensity spectrum, and the amplitude of the field maximum are maximal. At shell thicknesses, when the WGM field is partly located in the core and partly in the shell, the running wave is reflected from both boundaries, and both of them participate in the mode formation. As the shell thickness increases, the WGM field gradually transfers into the shell (Fig. 6), the role of the core-shell boundary gradually decreases, and the role of the shell-air boundary in the mode formation increases. Due to the disappearance of the reflection from the core-shell boundary and due to the lower reflection coefficient of the shell-air boundary, the WGM width increases, the peaks amplitudes

in the emission spectrum and the radial field distribution maximum decrease.

The width and quality factor have a complex dependence on the thickness, which is associated with a gradual transition of the WGM field from the core to the shell. In this case, the width of TM-polarized modes is always greater, than the width of TE-polarized modes, and the quality factor of TE-polarized modes is always greater, than the quality factor of TM-polarized modes in the entire range of investigated thicknesses (Fig. 7, *b, c*). In the 600 nm thickness region, an almost linear increase in the wavelength and mode width is observed (Fig. 7, *a, b*). In this region of thicknesses, the quality factor saturates and becomes practically constant.

The difference between the wavelengths of TE- and TM-polarized WGMs with the same indices l and q differs noticeably for different thicknesses (Fig. 5). Figure 7, *d* shows the calculated dependence of the relative difference between the wavelengths of the TE^1_{27} and TM^1_{27} modes on the shell thickness. The dependence has a noticeable minimum (Fig. 7, *d*) at a shell thickness of 250 nm. At this thickness, the maximum of the TE^1_{27} mode electric field transfers from the core to the shell (Fig. 6, *d*). For shell thicknesses greater, than 600 nm the magnitude of the relative wavelength difference saturates. We note, that for plane waves the minimum of the relative difference between TE- and TM-polarized eigenmodes wavelengths was found earlier in planar microcavities with distributed Bragg reflectors [59].

Absorption in the shell material can have a strong effect on the WGM parameters and on the type of the radiation spectrum. Figure 8 shows the emission spectra of the shell at different values of absorption, which is given by the imaginary part of the permittivity of the shell material. The calculation was carried out for a 300 nm luminescent shell with a complex refraction index of the shell surrounding a core with a diameter of 6 μm and a refraction index of 1.46. The real part of the complex permittivity of the shell is 1.72, the imaginary part varies within the range of 0–0.05.

An increase in the absorption in the shell leads to a decrease in the amplitude of the WGM peaks and to their broadening, while the spectral position of the peaks does not change. Absorption has a different effect on modes with different radial indices. An increase in the imaginary part of the permittivity from 0 to 0.001 leads to a sharp decrease in the amplitude and broadening of the WGM peaks with a radial index $q = 1$, while the peak amplitudes of the modes with a radial index $q = 2$ decrease much more weakly (Fig. 8, *a–c*).

At the value of permittivity imaginary part equal to 0.01, the WGM peaks with radial index $q = 1$ almost completely disappear, and the peaks of modes with the radial index $q = 2$ are still observed in the spectrum, but their amplitude becomes much smaller, than in the absence of absorption, and the peaks themselves are broadened (Fig. 8, *d*). Thus, the absorption in the shell completely suppresses the modes with $q = 1$. When the permittivity imaginary part is 0.05,

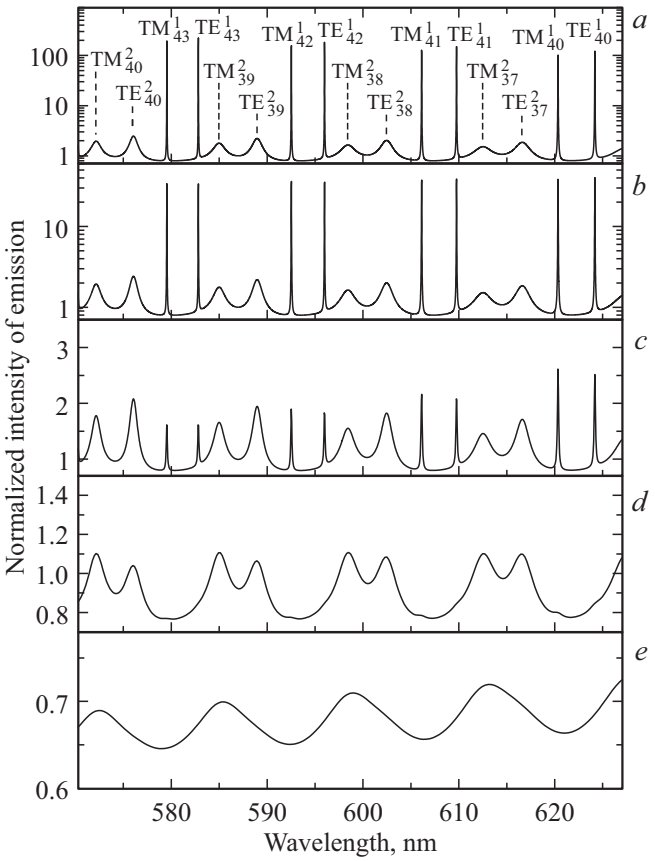

Figure 8. Spectral dependences of the radiation intensity of non-polarized radiation of the 300 nm luminescent shell surrounding a core with a diameter of 6 μm and refraction index of 1.46. The real part of the complex permittivity of the shell is 1.72, the imaginary part is 0 (*a*), 0.0001 (*b*), 0.001 (*c*), 0.01 (*d*), 0.05 (*e*). Vertical dashed lines indicate WGM positions. The WGM designations are indicated above the peaks.

the peaks of the modes with the radial index $q = 2$ broaden so much, that they merge and become indistinguishable (Fig. 8, *e*).

It should also be noted, that at the value of permittivity imaginary part equal to 0.001, the amplitude of the WGM peaks with $q = 1$ decreases with increasing polar index (Fig. 8, *c*). At the value of the permittivity imaginary part equal to 0.01 (Fig. 8, *d*), the amplitudes of the TM peaks become larger, than the amplitudes of the TE peaks for the modes with $q = 2$, in contrast to the fact, that was at a lower value of the permittivity imaginary part within the range 0–0.001 (Fig. 8, *a–c*).

Thus, absorption in the shell has a different effect on WGMs with different polarizations, with different radial and polar indices, and also with different quality factors. By varying the absorption in the shell, one can select WGMs with different radial indices and suppress the highest quality modes.

Conclusion

In this study we simulated the emission spectra of core-shell microresonators, in which a luminescent shell with a lower refractive index than that of the core is deposited on a spherical optically transparent dielectric core of small diameter ($3.5-6\,\mu$m). The luminescence spectra of the shell and WGM electric field distribution along the radial coordinate were calculated using the expansion of the electromagnetic wave field in the basis of vector spherical harmonics and the method of spherical wave transfer matrices. For each polarization (TE and TM), the luminescence spectrum consists of a large number of ordered peaks corresponding to the WGM.

The dependences of the luminescence spectra on the value of the refraction index of the shell and the core diameter are studied. It is shown, that an increase in the shell refraction index and core diameter leads to a decrease in the width and an increase in the WGM quality factor, to a mode shift to the long-wavelength region of the spectrum, and to the appearance of modes with a radial index $q = 2$ in the spectrum.

The dependence of WGM parameters (wavelength, width, quality factor) and radial distribution of the electric field strength of modes on the shell thickness is studied. It is shown, that as the shell thickness increases, the amplitudes of the peaks in the luminescence spectrum and the values of maxima of WGM electric field distribution along the radial coordinate decrease. With an increase in the shell thickness, the WGM field gradually passes from the core to the shell, since it is at the outer boundary of the shell that the electromagnetic wave undergoes total internal reflection, and this boundary plays a key role in the WGM formation. In this case, the role of the core-shell boundary in the formation of modes decreases.

The dependence of the relative difference between the wavelengths of TE and TM polarized modes with the same polar and radial indices on the shell thickness is considered. It is found that this value has a minimum at the value of the shell thickness, at which the maximum of the radial distribution of the electric field strength of the mode passes from the core to the shell.

The dependence of the luminescence spectra on the shell absorption value has been studied. An increase in the absorption in the shell, which is specified by the imaginary part of the shell material permittivity, leads to a decrease in the amplitude and broadening of the peaks, corresponding WGM, while the spectral position of the peaks does not change. It is shown, that the absorption has a different effect on the peaks in the luminescence spectrum depending on the quality factor, polarization, polar and radial mode indices. As absorption increases, the peaks in the luminescence spectrum corresponding to high-quality modes with radial index $q = 1$ can be completely suppressed, while the peaks corresponding to low-quality modes with radial index $q = 2$ will still be present in the spectrum.

Funding

The study was carried out using state budget funds on the topic of state assignment 0040-2019-0012.

Conflict of interest

The authors declare that they have no conflict of interest.

References

[1] *Oraevsky A.N.* // Quantum Electron. 2002. V. 32. N 5. P. 377. doi 10.1070/QE2002v032n05ABEH002205
[2] *Gorodetsky M.L.* Opticheskie mikrorezonatory s gigantskoj dobrotnost'yu (in Russian). M.: FIZMATLIT, 2011. 416 p. (in Russian)
[3] *Foreman M.R., Swaim J.D., Vollmer F.* // Adv. Opt. Photon. 2015. V. 7. N 2. P. 168. doi 10.1364/AOP.7.000168
[4] *François A., Zhi Y., Meldrum A.* // Photonic Materials for Sensing, Biosensing and Display Devices. Springer International Publishing, 2016. V. 229. P. 237. doi 10.1007/978-3-319-24990-2
[5] *Ward J., Benson O.* // Las. Photon. Rev. 2011. V. 5. N 4. P. 553. doi 10.1002/lpor.201000025
[6] *Chiasera A., Dumeige Y., Féron P., Ferrari M., Jestin Y., Nunzi Conti G., Pelli S., Soria S., Righini G.C.* // Las. Photon. Rev. 2010. V. 4. N 3. P. 457 doi 10.1002/lpor.200910016
[7] *Rakovich Y.P., Donegan J.F.* // Las. Photon. Rev. 2010. V. 4. N 2. P. 179. doi 10.1002/lpor.200910001
[8] *Righini G.C., Soria S.* // Sensors. 2016. V. 16. N 6. P. 905. doi 10.3390/s16060905
[9] *Cai L., Pan J., Zhao Y., Wang J., Xiao S.* // Phys. Stat. Sol. A. 2020. V. 217. N 6. P. 1900825. doi 10.1002/pssa.201900825
[10] *Venkatakrishnarao D., Mamonov E.A., Murzina T.V., Chandrasekar R.* // Adv. Opt. Mater. 2018. V. 6. N 18. P. 1800343. doi 10.1002/adom.201800343
[11] *Gorodetskii M.L., Ilchenko V.S., Savchenkov A.A.* // Opt. Lett. 1996. V. 21. N 7. P. 453. doi 10.1364/OL.21.000453
[12] *Reynolds T., Riesen N., Meldrum A., Fan X., Hall J.M.M., Monro T.M., François A.* // Las. Photon. Rev. 2017. V. 11. N 2. P. 1600265. doi 10.1002/lpor.201600265
[13] *Vollmer F., Arnold S.* // Nat. Methods. 2008. V. 5. N 7. P. 591. doi 10.1038/NMETH.1221
[14] *Jiang X., Qavi A.J., Huang S.H., Yang L.* // Matter. 2020. V. 3. N 2. P. 371. doi 10.1016/J.MATT.2020.07.008
[15] *Zhi Y., Yu X.-C., Gong Q., Yang L., Xiao Y.-F.* // Adv. Mater. 2017. V. 29. N 12. P. 1604920. doi 10.1002/adma.201604920
[16] *Toropov N., Cabello G., Serrano M.P., Gutha R.R., Rafti M., Vollmer F.* // Light Sci. Appl. 2021. V. 10. P. 42. doi 10.1038/s41377-021-00471-3
[17] *Toropov N., Vollmer F.* // Light Sci. Appl. 2021. V. 10. P. 77. doi 10.1038/s41377-021-00517-6
[18] *Weller A., Liu F.C., Dahint R., Himmelhaus M.* // Appl. Phys. B. 2008. V. 90. N 3-4. P. 561. doi 10.1007/s00340-007-2893-2
[19] *Himmelhaus M., Krishnamoorthy S., Francois A.* // Sensors. 2010. V. 10. N 6. P. 6257. doi 10.3390/s100606257
[20] *Monte A.F.G., Rabelo D., Morais P.C.* // J. All. Comp. 2010. V. 495. N 2. P. 436. doi 10.1016/j.jallcom.2009.11.040
[21] *Dantham V.R., Bisht P.B.* // J. Opt. Soc. Am. B. 2009. V. 26. N 2. P. 290. doi 10.1364/JOSAB.26.000290

[22] *Mamonov E.A., Maydykovskiy A.I., Mitetelo N.V., Venkatakrishnarao D., Chandrasekar R., Murzina T.V.* // Laser Phys. Lett. 2018. V. 15. N 3. P. 035401. doi 10.1088/1612-202x/aa9b23
[23] *Venkatakrishnarao D., Sahoo C., Vattikunta R., Annadhasan M., Naraharisetty S.R.G., Chandrasekar R.* // Adv. Opt. Mater. 2017. V. 5. N 22. P. 1700695. doi 10.1002/adom.201700695
[24] *Möller B., Artemyev M.V., Woggon U., Wannemacher R.* // Appl. Phys. Lett. 2002. V. 80. N 18. P. 3253. doi 10.1063/1.1475364
[25] *Götzinger S., Menezes L. de S., Benson O., Talapin D.V., Gaponik N., Weller H., Rogach A.L., Sandoghdar V.* // J. Opt. B: Quantum Semiclass. Opt. 2004. V. 6. N 2. P. 154. doi 10.1088/1464-4266/6/2/005
[26] *Fan X., Palinginis P., Lacey S., Wang H., Lonergan M.C.* // Opt. Lett. 2000. V. 25. N 21. P. 1600. doi 10.1364/OL.25.001600
[27] *Finlayson C.E., Sazio P.J.A., Sanchez-Martin R., Bradley M., Kelf T.A., Baumberg J.J.* // Semicond. Sci. Technol. 2006. V. 21. N 3. P. L21. doi 10.1088/0268-1242/21/3/L01
[28] *Melnikau D., Savateeva D., Chuvilin A., Hillenbrand R., Rakovich Y.P.* // Opt. Expr. 2011. V. 19. N 22. P. 22280. doi 10.1364/OE.19.022280
[29] *Mi Y., Zhang Z., Zhao L., Zhang S., Chen J., Ji Q., Shi J., Zhou X., Wang R., Shi J., Du W., Wu Z., Qiu X., Zhang Q., Zhang Y., Liu X.* // Small. 2017. V. 13. N 42. P. 1701694. doi 10.1002/smll.201701694
[30] *Schietinger S., Schröder T., Benson O.* // Nano Lett. 2008. V. 8. N 11. P. 3911. doi 10.1021/nl8023627
[31] *Rakovich Y.P., Yang L., McCabe E.M., Donegan J.F., Perova T., Moore A., Gaponik N., Rogach A.* // Semicond. Sci. Technol. 2003. V. 18. N 11. P. 914. doi 10.1088/0268-1242/18/11/302
[32] *Eurov D.A., Stovpiaga E.Yu., Kurdyukov D.A., Dukin A.A., Smirnov A.N., Golubev V.G.* // Phys. Solid State. 2020. V. 62. N 10. P. 1898. doi 10.1134/S1063783420100054
[33] *Grudinkin S.A., Dontsov A.A., Feoktistov N.A., Baranov M.A., Bogdanov K.V., Averkiev N.S., Golubev V.G.* // Semiconductors. 2015. V. 49. N 10. P. 1369. doi 10.1134/S1063782615100085
[34] *Teraoka I., Arnold S.* // J. Opt. Soc. Am. B. 2007. V. 24. N 3. P. 653. doi 10.1364/JOSAB.24.000653
[35] *Zijlstra P., van der Molen K.L., Mosk A.P.* // Appl. Phys. Lett. 2007. V. 90. N 16. P. 161101. doi 10.1063/1.2722695
[36] *Pang S., Beckham R.E., Meissner K.E.* // Appl. Phys. Lett. 2008. V. 92. N 22. P. 221108. doi 10.1063/1.2937209
[37] *Francois A., Himmelhaus M.* // Sensors. 2009. V. 9. N 9. P. 6836. doi 10.3390/s90906836
[38] *Beier H.T., Coté G.L., Meissner K.E.* // Ann. Biomed. Eng. 2009. V. 37. N 10. P. 1974. doi 10.1007/s10439-009-9713-2
[39] *Trofimova E.Y., Aleksenskii A.E., Grudinkin S.A., Korkin I.V., Kurdyukov D.A., Golubev V.G.* // Colloid J. 2011. V. 73. N 4. P. 546. doi 10.1134/S1061933X11040156
[40] *Trofimova E.Yu., Kurdyukov D.A., Yakovlev S.A., Kirilenko D.A., Kukushkina Yu.A., Nashchekin A.V., Sitnikova A.A., Yagovkin M.A., Golubev V.G.* // Nanotechnol. 2013. V. 24. N 15. P. 155601. doi 10.1088/0957-4484/24/15/155601
[41] *Kurdyukov D.A., Eurov D.A., Kirilenko D.A., Kukushkina J.A., Sokolov V.V., Yagovkina M.A., Golubev V.G.* // Micro. Mesopor. Mater. 2016. V. 223. P. 225. doi 10.1016/j.micromeso.2015.11.018
[42] *Kurdyukov D.A., Eurov D.A., Kirilenko D.A., Sokolov V.V., Golubev V.G.* // Micro. Mesopor. Mater. 2018. V. 258. P. 205. doi 10.1016/j.micromeso.2017.09.017
[43] *Trofimova E.Yu., Grudinkin S.A., Kukushkina Yu.A., Kurdyukov D.A., Medvedev A.V., Yagovkina M.A., Golubev V.G.* // Phys. Solid State. 2012. V. 54. N 6. P. 1298. doi 10.1134/S1063783412060339
[44] *Cho E.-B., Volkov D.O., Sokolov I.* // Small. 2010. V. 6. N 20. P. 2314. doi 10.1002/smll.201001337
[45] *Kalaparthi V., Palantavida S., Sokolov I.* // J. Mater. Chem. C. 2016. V. 4. N 11. P. 2197. doi 10.1039/c5tc04221f
[46] *Nelson D.K., Razbirin B.S., Starukhin A.N., Eurov D.A., Kurdyukov D.A., Stovpiaga E.Yu., Golubev V.G.* // Opt. Mater. 2016. V. 59. P. 28. doi 10.1016/j.optmat.2016.03.051
[47] *Eurov D.A., Kurdyukov D.A., Medvedev A.V., Kirilenko D.A., Tomkovich M.V., Golubev V.G.* // Nanotechnol. 2021. V. 32. N 21. P. 215604. doi 10.1088/1361-6528/abe66e
[48] *Sathe T.R., Agrawal A., Nie S.* // Anal. Chem. 2006. V. 78. N 16. P. 5627. doi 10.1021/ac0610309
[49] *Eurov D.A., Kurdyukov D.A., Kirilenko D.A., Kukushkina Yu.A., Nashchekin A.V., Smirnov A.N., Golubev V.G.* // J. Nanopart. Res. 2015. V. 17. N 2. P. 82. doi 10.1007/s11051-015-2891-y
[50] *Ushakova E.V., Cherevkov S.A., Sokolova A.V., Li Y., Azizov R.R., Baranov M.A., Kurdyukov D.A., Stovpiaga E.Y., Golubev V.G., Rogach A.L., Baranov A.V.* // Chemnanomat. 2020. V. 6. N 7. P. 1080. doi 10.1002/cnma.202000154
[51] *Stepanidenko E.A., Khavlyuk P.D., Arefina I.A., Cherevkov S.A., Xiong Y., Döring A., Varygin G.V., Kurdyukov D.A., Eurov D.A., Golubev V.G., Masharin M.A., Baranov A.V., Fedorov A.V., Ushakova E.V., Rogach A.L.* // Nanomaterials. 2020. V. 10. N 6. P. 1063. doi 10.3390/nano10061063
[52] *Cherevkov S., Azizov R., Sokolova A., Nautran V., Miruschenko M., Arefina I., Baranov M., Kurdyukov D., Stovpiaga E., Golubev V., Baranov A., Ushakova E.* // Nanomaterials. 2021. V. 11. N 1. P. 119. doi 10.3390/nano11010119
[53] *Kurdyukov D.A., Eurov D.A., Medvedev A.V., Golubev V.G.* // Tech. Phys. Lett. 2020. V. 46. N 9. P. 928. doi 10.1134/S1063785020090229
[54] *Tang F., Li L., Chen D.* // Adv. Mater. 2012. V. 24. N 12. P. 1504. doi 10.1002/adma.201104763
[55] *Colilla M., González B., Vallet-Regí M.* // Biomater. Sci. 2013. V. 1 N 2. P. 114. doi 10.1039/C2BM00085G
[56] *He Q., Shi J.* // Adv. Mater. 2014. V. 26. N 3. P. 391. doi 10.1002/adma.201303123
[57] *Hall J.M.M., Reynolds T., Henderson M.R., Riesen N., Monro T.M., Shahraam Afshar V.* // Opt. Expr. 2017. V. 25. N 6. P. 6192. doi 10.1364/OE.25.006192
[58] *Righini G.C., Dumeige Y., Féron P., Ferrari M., Nunzi Conti G., Ristic D., Soria S.* // Nuovo Cimento. 2011. V. 34. N 7. P. 435. doi 10.1393/ncr/i2011-10067-2
[59] *Dukin A.A., Feoktistov N.A., Golubev V.G., Medvedev A.V., Pevtsov A.B., Sel'kin A.V.* // Phys. Rev. E. 2003. V. 67. N 4. P. 046602. doi 10.1103/PhysRevE.67.046602